AIP | The Journal of Chemical Physics

Modeling high-temperature diffusion of gases in micro and mesoporous amorphous carbon

Raghavan Ranganathan, Srujan Rokkam, Tapan Desai, Pawel Keblinski, Peter Cross, and Richard Burnes

Citation: The Journal of Chemical Physics **143**, 084701 (2015); doi: 10.1063/1.4928633
View online: http://dx.doi.org/10.1063/1.4928633
View Table of Contents: http://scitation.aip.org/content/aip/journal/jcp/143/8?ver=pdfcov
Published by the AIP Publishing

Modeling high-temperature diffusion of gases in micro and mesoporous amorphous carbon

Raghavan Ranganathan,[1] Srujan Rokkam,[2,a)] Tapan Desai,[2] Pawel Keblinski,[1]
Peter Cross,[3] and Richard Burnes[3]
[1]*Department of Materials Science and Engineering, Rensselaer Polytechnic Institute, Troy, New York 12180, USA*
[2]*Advanced Cooling Technologies, Inc., 1046 New Holland Ave., Lancaster, Pennsylvania 17601, USA*
[3]*Naval Air Warfare Center, 1900 Knox Road, China Lake, California 93555, USA*

(Received 2 February 2015; accepted 4 August 2015; published online 24 August 2015)

In this work, we study diffusion of gases in porous amorphous carbon at high temperatures using equilibrium molecular dynamics simulations. Microporous and mesoporous carbon structures are computationally generated using liquid quench method and reactive force fields. Motivated by the need to understand high temperature diffusivity of light weight gases like H_2, O_2, H_2O, and CO in amorphous carbon, we investigate the diffusion behavior as function of two important parameters: (a) the pore size and (b) the concentration of diffusing gases. The effect of pore size on diffusion is studied by employing multiple realizations of the amorphous carbon structures in microporous and mesoporous regimes, corresponding to densities of 1 g/cm^3 and 0.5 g/cm^3, respectively. A detailed analysis of the effect of gas concentration on diffusion in the context of these two porosity regimes is presented. For the microporous structure, we observe that predominantly, a high diffusivity results when the structure is highly anisotropic and contains wide channels between the pores. On the other hand, when the structure is highly homogeneous, significant molecule-wall scattering leads to a nearly concentration-independent behavior of diffusion (reminiscent of Knudsen diffusion). The mesoporous regime is similar in behavior to the highly diffusive microporous carbon case in that diffusion at high concentration is governed by gas-gas collisions (reminiscent of Fickian diffusion), which transitions to a Knudsen-like diffusion at lower concentration. © *2015 AIP Publishing LLC.* [http://dx.doi.org/10.1063/1.4928633]

I. INTRODUCTION

Gas diffusion in porous media is a complex phenomenon that depends on various factors like pore size, pore morphology, concentration of diffusing gas, and temperature, among others. An understanding of the interplay of these factors has important implications for many applications like gas separation[1,2] and gas transport in porous media.[3–7] One of the earliest models for gas diffusion in porous media is the idealized, "dusty gas" model by Evans and Watson,[8] where the porous media was treated as giant dust molecules. Using kinetic theory, they gave a theoretical basis for the pressure-independent Knudsen diffusion and normal (Fickian) diffusion. However, diffusion in complex porous media is often not explained correctly using such idealized approximations.[9,10] Molecular simulations appear to be powerful tools to understand this complex phenomenon and it is possible to capture the dynamics of gas diffusion accurately.[11,12]

The diffusion characteristics are predominantly dictated by the pore size of the media. Porous solids are primarily classified as either microporous if the pore diameter is less than 2 nm or as mesoporous if it is between 2 and 50 nm.[3,13] The physics of diffusion in the context of micro and mesoporous diffusion is governed by the interplay of two kinds of molecular collisions, namely, (a) collisions between molecules and (b) collision between molecule and wall. Both mechanisms are, in general, expected to show distinctly different behavior depending on the pore size.[12] In general, a porous structure with a smaller pore size would have a greater ratio of molecule-wall collisions to molecule-molecule collisions, in comparison to structures with larger pore size. Adding another dimension to this interesting phenomenon is the effect of gas concentration (or alternately, the gas pressure assuming an ideal gas law) on diffusion. A general trend in this regard is the decrease in self-diffusivity with an increase in gas pressure as shown for diffusion in carbon nanotubes[4] and various crystalline materials like zeolites,[12,14] metal organic frameworks,[5] and silicalite. In some cases, unusual diffusional behavior arises due to special gas-gas or gas-wall interactions. For example, Krishna and van Baten[15] observed unusual diffusional behavior in silica mesopores due to molecular clustering. In general, the intermolecular and molecule-wall interactions together with the porous structure of the host solid play a complex role that needs to be understood to ascertain the diffusion characteristics.

Theoretical modeling of gas diffusion in porous media, particularly in amorphous materials has attracted significant attention over the years. MacElroy and Raghavan[16] studied diffusion of Lennard-Jones vapor (CH_4) in model microporous silica generated via a combination of Monte Carlo and molecular dynamics (MD) steps and estimated gas diffusivities that

a)Electronic mail: srujan.rokkam@1-act.com

agree reasonably with experiments. Sahimi and Jue[17] studied diffusion of molecules in model disordered porous media and found that diffusivity follows an exponential decay relation with the inverse of pore size. Lim *et al.*[18] probed diffusion of gases in an amorphous polymer (polyetherimide) and found that diffusion of gas molecules follows two kinds of motion, namely, oscillatory motions within the smaller cavities of the polymer and hopping from one cavity of the polymer matrix to another. Moore *et al.*[19] found that anomalous diffusion could occur at short time scales in disordered microporous carbon when molecules are trapped within pores. An interesting observation with regards to concentration dependence of gas diffusivity is that it could initially increase with gas pressure due to more molecules being able to diffuse through larger pores, followed by a transition to a decrease in diffusivity with concentration, arising from greater intermolecular collisions. Malek and Coppens[20] probed the effect of surface roughness of the matrix on gas diffusivity using Monte Carlo simulations and found that an increased roughness results in a decrease in self-diffusivity due to greater residence time of molecules on the surface, especially when the pores are narrow. More recently, Jiang *et al.*[21] used MD simulations to characterize dependence of gas selectivity on pore features (in particular, pore connectivity) in amorphous organic cages and found that diffusion in amorphous materials could be faster than its crystalline counterpart.

The focus of this work is to explain the characteristics of gas diffusion, and in particular, its dependence on gas concentration in microporous and mesoporous amorphous carbon structures. Amorphous carbon structures in the form of char are formed during pyrolysis of ablative materials used in heat-shield applications like solid rocket motor (SRM) nozzle. Understanding the diffusion characteristics of high temperature combustion edge gases in such structures is crucial to predict and optimize the performance of the heat-shield material used in SRM.

Gas diffusion, in general, can be categorized into three different types: (a) self-diffusivity, D_s arising from random migration of molecules in the absence of any concentration gradients, (b) transport diffusivity (or Fickian diffusivity) arising from presence of a concentration gradient (Fick's law), and (c) Maxwell-Stefan diffusivity that describes diffusion in presence of a mixture of gases with different chemical potentials. Simulation methodologies for obtaining the transport and Maxwell-Stefan diffusivities have been dealt with in detail by many researchers.[6,12,14,22,23] In the present work, we concentrate only on self-diffusivity of simple gas molecules in amorphous micro and mesoporous carbon using equilibrium molecular dynamics simulations. We are mainly concerned with high-temperature diffusion of single component species where adsorption plays a negligible role and thus primarily deals with self-diffusivities. This scenario is of direct consequence for interaction of gases with carbonaceous materials like ablatives[24] and solid fuels.[25] We consider amorphous carbon structures at two different densities of 0.5 g/cm^3 and 1 g/cm^3 with pore sizes in the meso and microporous regimes, respectively. From an analysis of molecular collisions, diffusion trajectories, and calculated self-diffusivities, we explain the dependence of diffusivity on gas concentration and the pore features. Further, to ascertain the influence of randomness in amorphous structures, we investigate the diffusion behavior of H_2 gas in multiple realizations of the mesoporous and microporous regimes.

The organization of this paper is as follows. In Section II, the simulation methodology consisting of the method of generation of porous structures used for diffusion simulations and the computational framework for diffusion analysis is presented. Results for the characteristics of diffusion in micro and mesoporous amorphous carbon are described in Section III. Using multiple realizations of the two porous structures, our key finding is that diffusion in mesoporous carbon is highly anisotropic due to presence of large diffusion channels, which leads to diffusivities that are one order of magnitude larger than that in microporous carbon. For microporous carbon, two regimes of diffusion could exist—a "highly" diffusive structure that has wide channels for diffusion (similar to mesoporous carbon) or a "low" diffusion structure that has a highly homogeneous distribution of pore wall that leads to much lower diffusivities. Finally, the conclusions are presented in Section IV.

II. SIMULATION METHODOLOGY

A. Generation of porous carbon structures

The model carbon structures used in this study were generated using the liquid-quench method[26] and a reactive force field, ReaxFF.[27] The liquid quench method lends itself well to model amorphous structures, especially amorphous carbon,[28–30] gels,[31] and inorganic oxides.[32] ReaxFF is a reactive potential, which uses the concept of bond order to model the chemical interactions within a reactive system. The bond order based definition of atomic and molecular interactions excludes the need for predefined reactive sites (or reaction pathways) and allows for description of dynamic bond breaking and formation. The ReaxFF force field parameters are derived solely from quantum mechanics and provide an unbiased representation of the reaction chemistry. Thus, ReaxFF potentials can be directly applied to novel systems that may not have been studied experimentally. Using the liquid quench method in conjunction with ReaxFF allows us to effectively model various amorphous carbon structures across a wide variety of densities, encompassing char to glassy carbon to diamond-like carbon. The steps involved in the overall process are (a) start with carbon atoms (~1200 atoms in total) at random positions in a periodic cell, ramp the temperature to a high value (10 000 K) and (b) a short equilibration at 10 000 K (15 ps) followed by (c) quenching the system to 3000 K over ~200 ps. Following this, the system was (d) annealed at 3000 K for 200 ps and finally (e) quenched and equilibrated at 300 K. We used the ReaxFF force field for hydrocarbons[33] that has been used successfully to model reactions in various forms of carbon like graphene[34] and carbon nanotubes.[35] Since ReaxFF is computationally expensive, we are limited by the total simulation times for reasonably large structures. The current simulation time-spans yield reasonable models of amorphous carbon for both mesoporous and microporous regimes to study the effect of porosity on diffusion and do not have a direct bearing with any physical process. Such

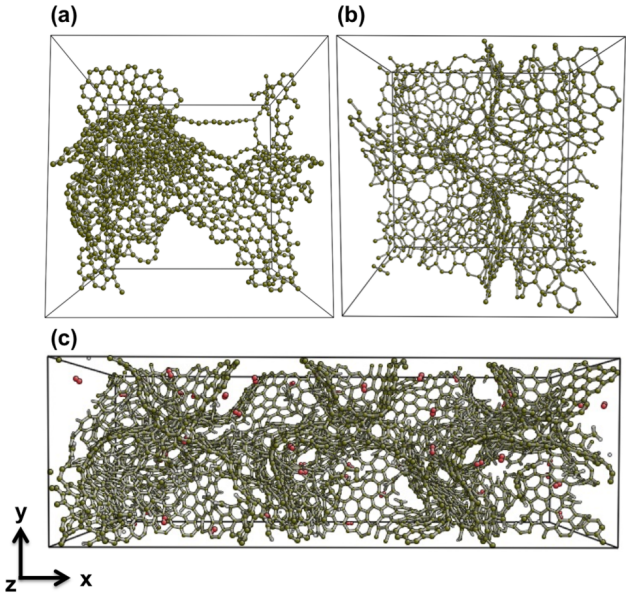

FIG. 1. Snapshots of (a) 0.5 g/cm^3 mesoporous carbon, (b) 1 g/cm^3 microporous carbon, and (c) triply replicated and H-passivated 1 g/cm^3 char with 50 O_2 molecules (O_2 shown in red). Structures were generated using the liquid-quench method with the ReaxFF potential.

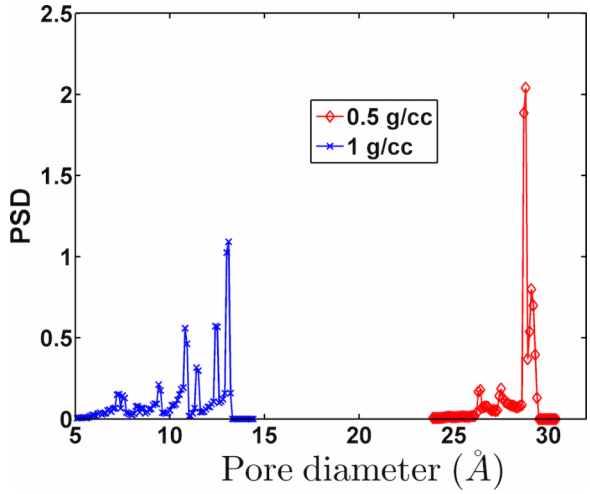

FIG. 2. Pore size distribution for a 0.5 g/cm^3 (mesoporous) carbon structure and a 1 g/cm^3 (microporous) carbon structure, as calculated using the Zeo++ code.

fast quench rate has been routinely employed in simulations to keep computational time feasible.[28,36] The temperatures and simulation protocol chosen were similar to the work of Shi[30] who used the liquid quench method with the RSS reactive potential to model amorphous carbon.

Two representative structures for the two densities of 0.5 g/cm^3 and 1 g/cm^3 are shown in Figures 1(a) and 1(b), respectively. For both structures, the system comprised of about 1200 carbon atoms with the predominant hybridization being sp^2 (~85%). Our amorphous carbon models exhibit similar structural features as compared to a multitude of models from the literature.[29,30,37–39] As a final step in the structure generation, all unsatisfied valencies of carbon were passivated by addition of hydrogen atoms. To characterize these amorphous carbon structures, a brief discussion on their structural and pore features is provided below. A more detailed analysis of this scheme including structural and thermal characterizations of the carbon structures is a subject of a separate publication.[40]

To characterize the pore sizes of these model structures, we find the pore size distribution (PSD) using the tool Zeo++,[41] which uses Voronoi decomposition for describing the pore geometry. The Zeo++ code considers a probe molecule and bins the accessible pore diameters for the probe, into a histogram. In this work, we use a probe radius of 1.2 Å to find the PSD. Figure 2 shows the PSD for two sample structures—one 0.5 g/cm^3 and the other 1 g/cm^3, used in the present study.

In total, we generated six realizations of the mesoporous and eleven realizations of the microporous amorphous carbon (see the supplementary material[42] for visualization of the final structures). The average pore diameters of the 0.5 g/cm^3 and 1 g/cm^3 structures were found to be 2.706 ± 0.168 nm and 1.422 ± 0.166 nm, which fall under mesoporous and microporous regimes, respectively.[13] From the accessible volume of the two structures calculated using Zeo++, the porosity was found to be 0.639 ± 0.017 and 0.306 ± 0.020, respectively. Henceforth, these structures would be referred to as the mesoporous and microporous structure, respectively. We also note that the pores in both the micro and mesoporous structures are well connected with no inaccessible channels for the diffusing gases. Shown in Figure 3 are the accessible pore volumes (colored green) for one realization of microporous and mesoporous carbon computed using Zeo++. We find

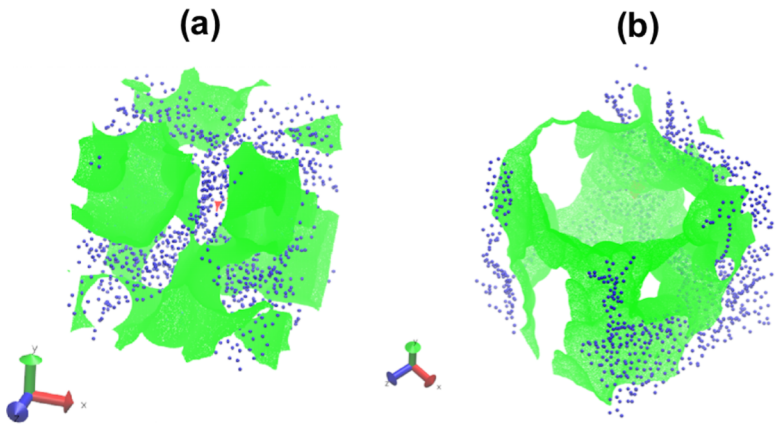

FIG. 3. Accessible pore volume (colored green) computed with a probe size of 1.2 Å using Zeo++ in (a) 1 g/cm^3 microporous carbon and (b) 0.5 g/cm^3 mesoporous case. The inaccessible pore volume is noted by a red volume, for example, a tiny speck at the center of 1 g/cm^3 case. The carbon atoms of the porous structure are shown in blue color. As seen, all the voids are well connected for providing diffusion channels for all the molecule sizes under consideration in this work.

that inaccessible pore volume is negligibly small for both the structures (as shown by a tiny red speck in the center of the microporous case). A probe radius of 1.2 Å was used such that the accessible volume is valid for all the gases considered. Thus, our structures do not prevent molecules from getting trapped in a certain pore indefinitely.

B. Model interaction parameters

Performing diffusion simulations of gases in these structures does not require use of reactive force field and thus, after the synthesis of the model structures, we switched to a much more computationally efficient, non-reactive, all-atom force field Polymer Consistent Force Field (PCFF).[43] This force field includes three and four-body angle and torsion interactions, in addition to bond-stretching and non-bonded Lennard-Jones (6-9) interactions. All two, three, and four body interaction terms were obtained from Ref. 43. The Lennard-Jones interaction parameters for like atom pairs are listed in Table I. The cutoff for non-bonded interactions was set as 10 Å and the hybridization of carbon was set as sp^2. We then introduce various gas species in a triply replicated, passivated structure as shown in Figure 1(c) for the case of 50 O_2 molecules in the 1 g/cm^3 structure. The replication step was to ensure sufficient statistics; since our structures are periodic, the choice of replication direction itself was found to not play any role in diffusion (diffusion coefficients calculated for different replication directions were found to differ by less than 1%). All simulations were performed using the LAMMPS code.[44]

C. Computational framework

Using MD simulations, the self-diffusivity D_s of various gases in micro and mesoporous carbon was calculated. Diffusion constant is usually calculated using two equivalent approaches: (a) integral of the velocity autocorrelation function (VACF) of the diffusing species and (b) slope of the mean-squared displacement (MSD) plotted as a function of time (Einstein's relationship). Both approaches are equivalent in the thermodynamic limit with enough statistics.[45] The corresponding formulae are given by Eqs. (1) and (2), respectively,

$$D_s(c) = \frac{1}{3}\int_0^\infty \langle v(0)\, v(t)\rangle\, dt, \tag{1}$$

$$D_s(c) = \frac{1}{6t}\left\langle |r(t) - r(0)|^2 \right\rangle. \tag{2}$$

In the present work, we have used the VACF method to calculate D_s. The complete shape of the VACF provides information about the nature of the atomistic dynamics, especially at the short time-scale regime, where back-scattering from the wall results in a negative "hump."

The simulation methodology involves equilibrating the entire system (carbon wall and gas molecules) initially in an NVT ensemble at the target temperature (350–1750 K) using a Berendsen thermostat (damping constant of 1 ps) for 1 ns. This was followed by production runs, where only porous material carbon atoms were thermostatted at the target temperature. The carbon wall is thus flexible, which is necessary to prevent the unphysical ballistic motion of molecules if the wall is completely rigid, especially at low gas concentrations, where diffusive motion arises only from gas-wall collisions.[46] Simulations were performed for about 0.5 ns for the highest gas concentration and for about 5 ns for the lowest concentration to achieve good convergence of the diffusion constants. A time step of 0.5 fs was used for all the simulations. Atomic velocity data were collected every 25 fs. Velocity of the center of mass of molecules was used in the computation of VACF. Such high-frequency data collection was sufficient for accurately capturing diffusion processes, considering that characteristic collision times were an order of magnitude larger. We used the Fast Fourier Transform (FFT) method[47] for efficiently computing the VACF.

An extensive set of simulations for gas diffusion in the 1 g/cm^3 structure (microporous) was carried out, where self-diffusion constants of the gases H_2, O_2, H_2O, and CO were calculated for four different temperatures of 350, 750, 1250, and 1750 K. The choice of these gases and temperatures was motivated in the context of amorphous carbon (such as char resulting from pyrolysis of ablative composites used in thermal protection systems) interacting with gases from atmosphere and oxidizing fuel (as in exhaust nozzle of the solid rocket motors).[48,49] The number of gas molecules considered are 10, 20, 50, 100, and 300 molecules such that, when normalized by the accessible volume, translates to gas concentration, c, ranging from about 1 kmol/m^3 to 22 kmol/m^3. For comparing the diffusion characteristics with the low-density (0.5 g/cm^3) mesoporous structure, similar simulations were performed with H_2 gas. Subsequently, both these cases are compared with diffusion in pure gas system. Finally, we consider diffusion of H_2 in multiple realizations of both micro and mesoporous structures to understand the effect of randomness of the amorphous structures. This entire set of system properties considered in order to understand the characteristics of diffusion in porous structures is given in Table II. It is to be noted that we focus on the high temperature regime where the effects of the gas adsorption and surface diffusion are negligible. This was

TABLE I. Non-bonded interaction parameters.

Atom pair	ε (kCal/mol)	σ (Å)
C–C	0.0640	4.010
H–H	0.0200	2.995
O–O	0.0600	3.535
C–H	0.0254	3.669
C–O	0.0578	3.809
O–H	0.0308	3.319

TABLE II. System parameters varied to study diffusion mechanisms of gases.

System	Gases considered	Temperature	Gas concentration
1 g/cm^3 (microporous carbon)	H_2, O_2, H_2O, CO	350–1750 K	1–22 kmol/m^3
0.5 g/cm^3 (mesoporous carbon)	H_2	350–1750 K	0.2–6 kmol/m^3
Free gas	H_2	350–1750 K	0.6–18 kmol/m^3

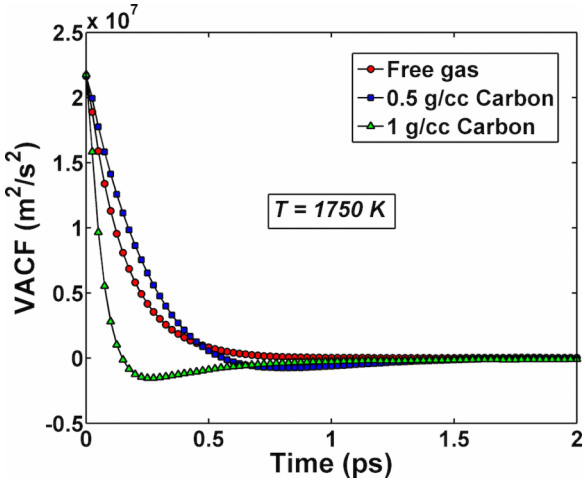

FIG. 4. Velocity autocorrelation function (VACF) plots for diffusion of 300 H_2 molecules in three different scenarios—(a) free gas diffusion (red circles), (b) 0.5 g/cm^3 mesoporous carbon (blue squares), and (c) 1 g/cm^3 microporous carbon (green triangles). The temperature under consideration is 1750 K.

verified by computing the radial distribution function between carbon and gas atoms, during the diffusion simulation. We observe no local ordering even for the highest concentration and lowest temperature (350 K) used in this study. In fact, the carbon-gas interaction needs to be increased by 8 times from our standard value to start observing adsorption effects (see the supplementary material[42] for more details).

III. RESULTS AND DISCUSSION

A. Characteristics of diffusion in porous material

In this section, the effect of gas concentration on gas diffusion in meso and microporous material is discussed. Diffusion constants were calculated using the VACF method for various gas concentrations and temperature (as given in Table II) for three cases—(a) diffusion in 1 g/cm^3 (microporous) carbon, (b) diffusion in 0.5 g/cm^3 (mesoporous) carbon, and for a comparative study, (c) diffusion of free gas in the absence of any external media. The characteristic diffusion mechanisms are expected to be quite different for the three cases due to the additional scattering effect due to the presence of the porous carbon matrix. In the presence of carbon wall, the molecules typically collide with the wall, in addition to inter-molecular collision. This is reflected in the behavior of the VACF, as shown in Figure 4, evaluated for 300 H_2 molecules (corresponding to the highest gas concentration considered) at 1750 K for all the three cases. The microporous (1 g/cm^3) structure leads to an extremely fast decay of the VACF as compared to the other two cases. In fact, the VACF exhibits a negative hump which is associated with back-scattering of molecules from the carbon wall, similar to the results of MacElroy and Raghavan[16] for the case of diffusion in microporous silica. In the case of mesoporous structure, the negative hump is less pronounced and occurs at later times. The free gas case on the other hand does not show a negative hump.

The converged value of the running integral of VACF gives the self-diffusion coefficient according to Eq. (2). Such a sample running integral plot for diffusion of 300 H_2 molecules in microporous carbon is shown in Figure 5. As can be seen in Figure 5(a), good convergence in the running integral was typically seen within roughly 30 ps for the highest concentration (containing 300 molecules) and about 100 ps for the lowest concentration (with 10 molecules) considered. Figure 5(b) shows the initial portion of the running integral where a characteristic peak appears that corresponds to the negative hump of the VACF. We call the position of this peak, the characteristic time, τ_c, for the average duration spent by a molecule before colliding with the wall. A well-defined τ_c was obtained for diffusion of all the four gases (H_2, O_2, CO, and H_2O) in microporous carbon. For mesoporous carbon, on the other hand, the gas-wall collision was much less prominent as seen in Figure 6, where the running integral for the lowest and highest gas concentrations is shown for various temperatures. The peak corresponding to τ_c was prominent only for large concentrations and at higher temperatures. This indicates that the back-scattering effect from wall competes with intermolecular collisions at higher concentrations.

B. Diffusion in microporous structure

In this section, a detailed analysis of diffusion of gases (H_2, O_2, H_2O, and CO) in one realization of the 1 g/cm^3 microporous carbon structure is presented. Shown in Figure 7 is the concentration dependence of (a) diffusion constants (D) on the left panels and (b) the characteristic time (τ_c) on the right panels for all the four gases considered. In general, diffusion is expected to increase with decreasing concentration due to smaller scattering frequency and longer mean free paths. However, the observation is that D is largely independent of concentration. For the case of H_2 (Fig. 7(i-(a))), there is an

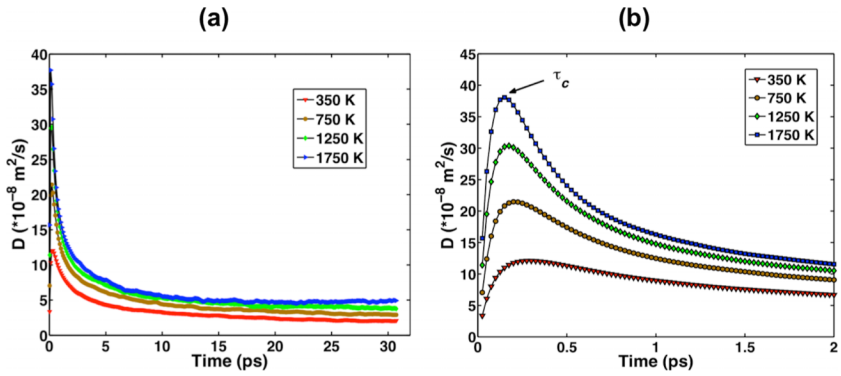

FIG. 5. (a) Running integral of VACF for the case of diffusion of 300 H_2 molecules in 1 g/cm^3 microporous carbon for a range of temperatures. (b) Initial portion of the running integral from part (a) shown magnified. The peak position corresponds to the characteristic time, τ_c for collision of molecules with the wall.

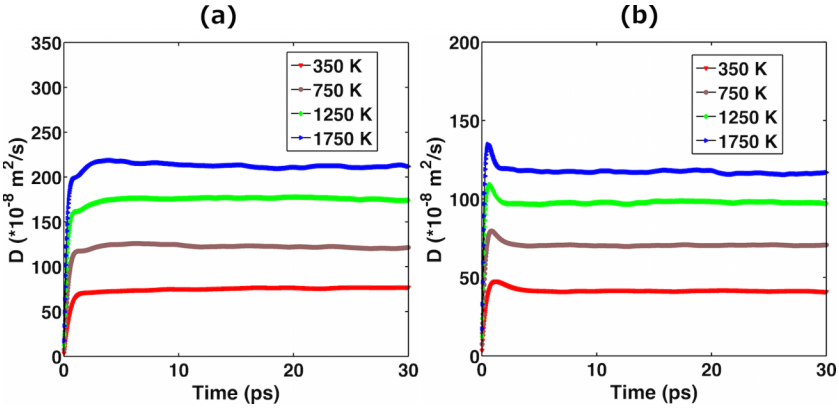

FIG. 6. Running integral of VACF in mesoporous carbon for various temperatures. (a) N = 10 molecules (corresponding to c = 0.18 kmol/m^3) and (b) N = 300 molecules (c = 5.54 kmol/m^3). The characteristic spike at τ_c is seen clearly only for the highest concentration (panel (b)).

initial sharp decrease in D followed by virtually no change in D with concentration. The relatively high diffusivity of H_2 at low concentration is not well understood at the moment. We speculate that new channels for pore-to-pore diffusion are opened at low concentrations as a consequence of significant reduction in intermolecular collisions. The magnitude of diffusivity, however, agrees well with the work of Jiang *et al.*,[21] who found the average self-diffusivity of H_2 in various amorphous carbon cage assemblies at density of 0.9 g/cm^3 to be about 1.7×10^{-8} m^2/s at 300 K. For O_2 (Fig. 7(ii-(a))), we found that D actually increases gradually with c. This is a distinctly different behavior for concentration dependence in that the presence of an external microporous matrix could actually lead to an increase in diffusivity with concentration. This was also observed in diffusion of small hydrocarbons in mesoporous silica[15] and the reason for this behavior was attributed to molecular clustering. Both H_2O (Fig. 7(iii-(a))) and CO (Fig. 7(iv-(a))) show an almost constant diffusivity with increasing concentration. The nearly concentration-independence of diffusivity arises from the microporous nature of wall that leads to significant gas-wall collisions.

Figure 7 (right panels) also shows the variation of the characteristic time, τ_c as a function of concentration. We observe that in general, τ_c decreases almost monotonically with increasing concentration for all the four gases. This is due to quicker gas-wall collisions arising from a higher frequency of gas-gas collisions at higher concentrations. τ_c is seen to be of the order of 1 ps for O_2, H_2O, and CO and about 0.2–0.4 ps for H_2, depending on the temperature.

To capture the combined effect of temperature and the gas pressure (which depends on the gas concentration) on diffusion, we construct three-dimensional "diffusion maps" that are surface plots of D as a function of temperature and pressure. Shown in Figure 8 are the diffusion maps for the four different gases diffusing in microporous carbon. The gas pressure was computed from the ideal gas law,

$$PV_{\text{free}} = NRT, \tag{3}$$

where the volume, V_{free} is the free, porous volume available for the diffusing gases. Increasing temperature was seen to increase D, with the maximum increase going from 350 K to 1750 K being typically about 2 times for H_2 and about 3-5 times for O_2, H_2O, and CO, depending on the concentration. Pressure on the other hand, being directly proportional to concentration, was seen to have a very negligible effect on D. For H_2, D is constant with decreasing pressure and it only increases for a very low pressure of ~3 atm (corresponding to 10 molecules). While O_2 showed a continuously decreasing diffusivity with pressure for all temperatures, H_2O and CO were seen to show negligible pressure dependence with small fluctuations at intermediate pressures. Diffusion maps such as these can aid in estimation of diffusivity at arbitrary intermediate temperatures and pressures by interpolation. We note that the diffusion behavior reported in Figure 7 corresponds to a unique 'low diffusion' regime. The classification of low and high diffusion regimes based on structural features is discussed in Section III C.

C. Effect of porosity and structural features

In Section III C 1, we characterize the diffusion behavior in microporous and mesoporous carbon and in Section III C 2, we report the structural aspects of the carbon matrix, which could lead to anisotropic diffusion in certain directions.

1. Diffusion in meso- and micro-porous carbon

Porosity of the matrix is expected to play a huge role in diffusion of gases. A mesoporous structure with larger pore size would lead to far fewer gas-wall collisions in comparison to a microporous structure. On the other hand, a mesoporous structure is still expected to show significantly lower diffusion than free gas where the only scattering mechanism is the intermolecular collisions. To compare the effect of pore structure on diffusion, we investigate the diffusion characteristics of H_2 gas at various gas concentrations and temperatures in three scenarios: (i) microporous carbon, (ii) mesoporous carbon, and (iii) free gas. An important consideration while comparing diffusivity across these structures is the need to obtain sufficient statistics by averaging across multiple realizations of the amorphous structure. We consider the case of H_2 diffusion at 750 K and 1750 K in a total of six distinct realizations of mesoporous carbon and eleven realizations of the microporous carbon structures, following the same simulation protocol to generate the structures as before. Simulations were also performed for the case of free gas (without the carbon matrix) at these concentrations and temperatures, for comparative purposes. The volume of simulation cell used for the free gas simulations was kept similar to the free volume, V_{free} in micro and mesoporous structures (refer Eq. (3)).

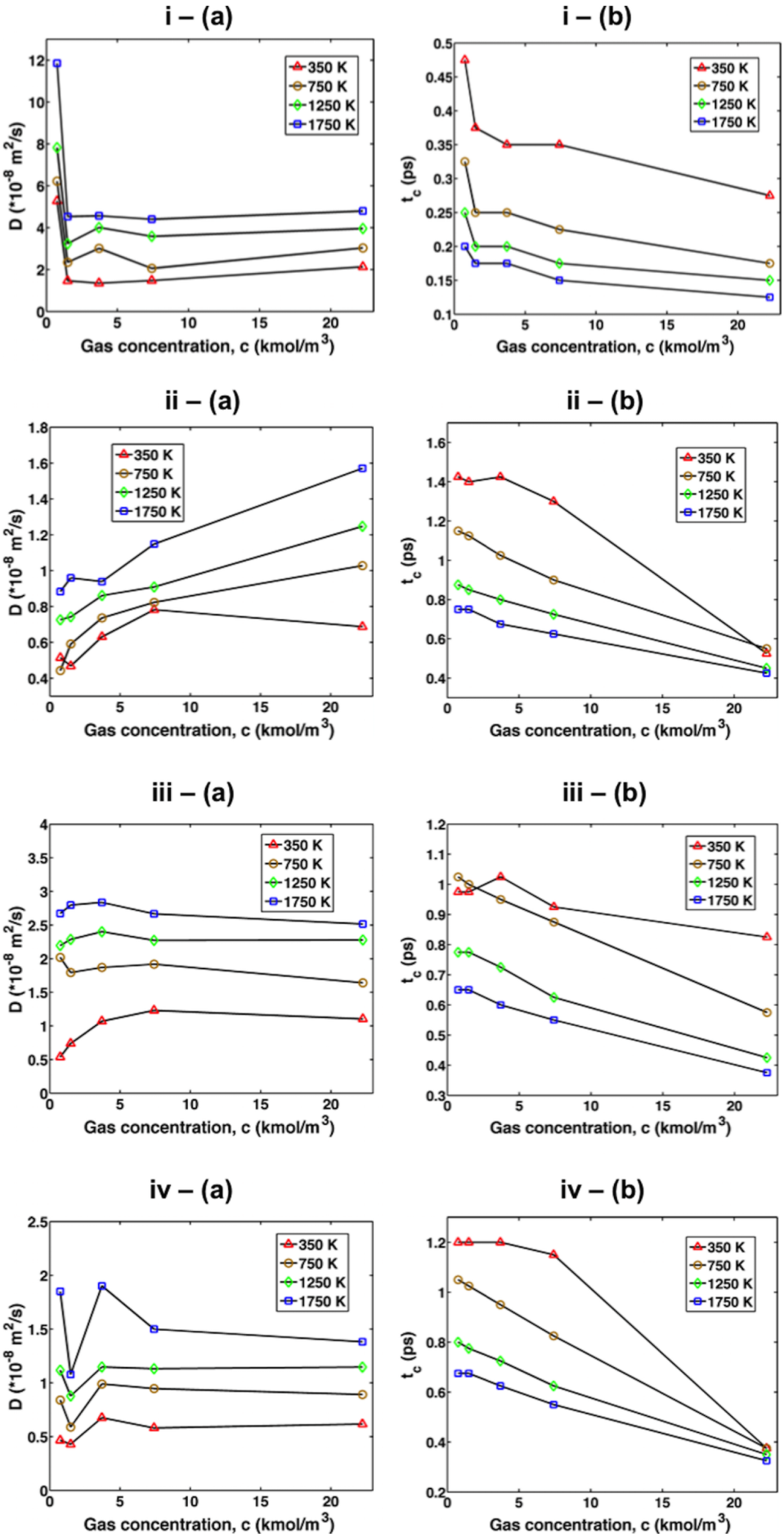

FIG. 7. Figures depicting diffusion behavior in 1 g/cm^3 microporous carbon. Self-diffusion constants (D) are plotted as a function of concentration (left, (a)) and characteristic time, τ_c for gas-wall collision is plotted as a function of concentration (right, (b)) for four different gases—(i)–H_2; (ii)–O_2; (iii)–H_2O, and (iv)–CO.

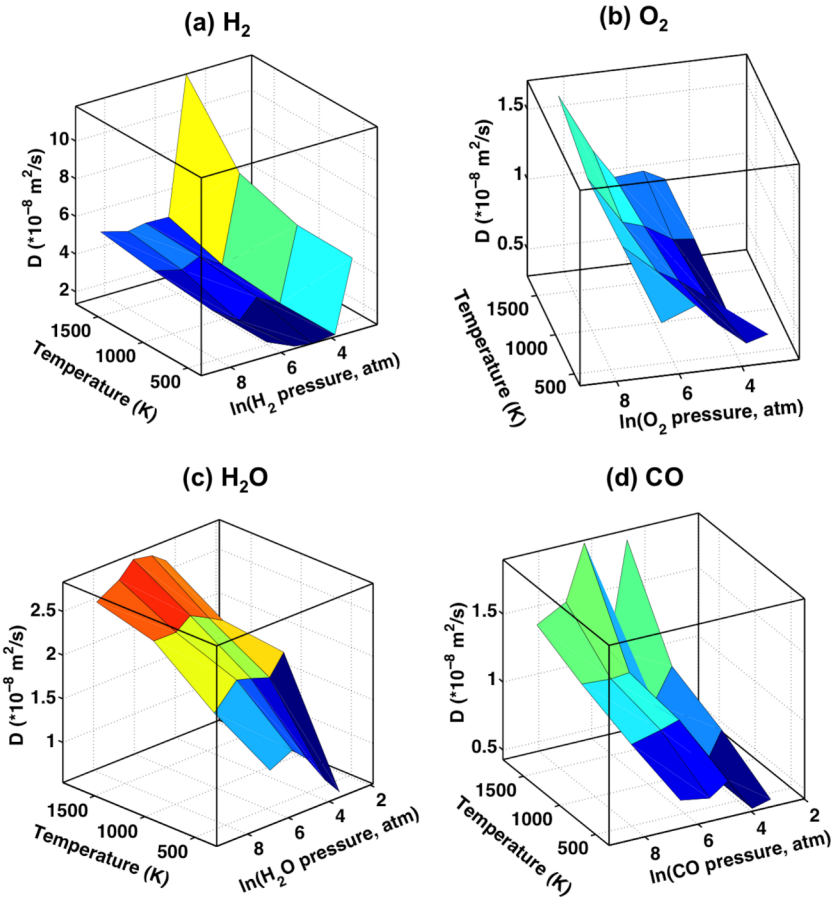

FIG. 8. Three-dimensional diffusion maps showing variation of diffusion constant (D) as a function of temperature and pressure for four different gases—(a) H_2, (b) O_2, (c) H_2O, and (d) CO for the case of 1 g/cm^3 microporous carbon.

The averaged diffusivities with the appropriate error bars for all these cases are presented as a function of inverse concentration, c^{-1} in Figure 9. For microporous diffusion, our model structures fall under two distinct diffusion regimes—they are either a "highly diffusive" structure as shown in panel (a) or a "low" diffusivity structure (panel (b)). The former case (highly diffusive) was seen to be the most prevalent with nine out of the eleven realizations corresponding to this case. As seen from the figure, the highly diffusive structure exhibits a 3 to 4 fold increase in diffusivity compared to the low diffusion structure. The latter case also shows negligible concentration dependence for diffusivity. On the other hand, the mesoporous structure was seen to exhibit an order of magnitude higher diffusivity (panel (c)) as compared to the microporous case. This is, however, still an order of magnitude lower diffusivity than the free gas case (panel (d)). More interesting to note is the dependence of D on concentration for the three cases. While the "low" diffusivity microporous carbon shows nearly concentration independent diffusivity except for very low concentration (at highest c^{-1} value, refer panel (b)), diffusion in the "highly" diffusive microporous carbon and mesoporous carbon was seen to strongly increase with decreasing concentration initially, followed by a gradual increase and saturation. The free gas case on the other hand shows a continuous linear increase in D with decreasing concentration.

It is well known that D is inversely proportional to concentration for pure gas diffusion arising from the inverse proportionality relation between mean free path and gas density and this was indeed verified by fitting a power law relation of the form $D = kc^{-n}$ for the data in Figure 9(d), where the exponent n was found to be very close to 1. For the mesoporous carbon case, the initial sharp increase in D with decreasing concentration is believed to be from a more free gas like behavior wherein inter-molecular collisions are more dominant than gas-wall collisions. This is a direct consequence of the larger pore volume as compared to the microporous carbon case. With a further decrease in concentration, however, the effect of gas-wall collisions increases and as a result, the concentration dependence significantly decreases akin to the "low" diffusion microporous carbon case.

2. *Influence of structural anisotropy*

Understanding concentration dependence of diffusion in the context of structural features of the matrix has been a classic problem explored in a variety of materials, most notably, in zeolites.[50] Quite a few studies have shown that the transport diffusivity (Fickian diffusion) in zeolite-gas systems could either increase, decrease, or remain independent of gas concentration depending on several factors.[14,50] Self-diffusivity, on the other hand, has been observed to increase with concentration only in systems which have strong gas adsorption (for example, gas diffusion in zeolites[51]) or relatively small pore sizes, where molecule-wall collisions are significant.[52] For the simulations presented in this work, gas adsorption is negligible (as noted in Section II C and supplementary material[42]). Thus, our results of decreasing self-diffusivity with increasing concentration for the case of mesoporous and "highly" diffusive micropo-

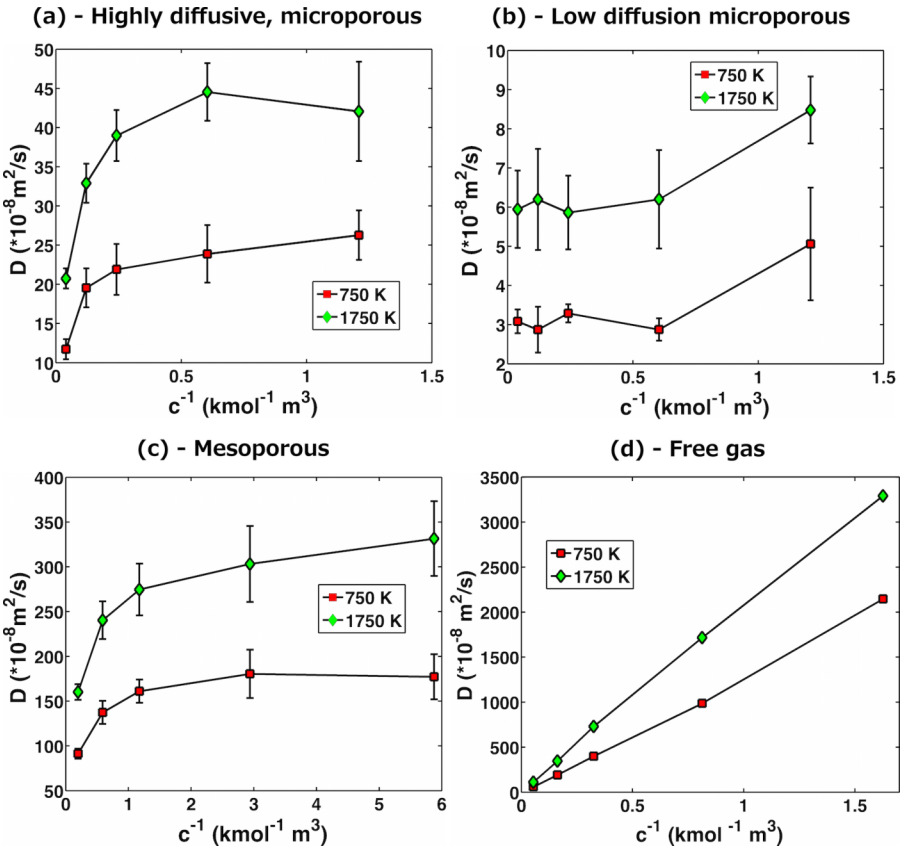

FIG. 9. Self diffusion constant plotted as a function of inverse concentration for the case of H_2 diffusing in (a) "highly" diffusive microporous carbon; (b) "low" diffusion microporous carbon; (c) mesoporous carbon; and (d) free gas at two temperatures. Length of error bars is equal to the standard deviation.

rous structures are consistent with the reported literature. For the "low" diffusion structure, as seen before, diffusivity is concentration-independent for a wide range of concentrations and increases only for very low concentration (Figure 9(c)). We attribute this to the effect of small pore sizes, where molecule-wall collisions are the predominant scattering mechanism.

To understand the observance of two diffusion regimes in microporous carbon, there is a need to assess the manifestation of structural features on the computed diffusivities. In general, pore-morphology and the manner in which pores are connected can significantly influence diffusion mechanisms. To ascertain the structural features responsible for these distinct concentration dependences, we compute the x, y, and z components of the VACF running integral separately for one representative structure for all three cases. These running integrals along with snapshots of the structure along the 3 axes are shown in Figure 10 for the case of mesoporous carbon. The projections of the atomic snapshots along the x, y, and z axes are denoted by the outward pointing vector symbol (⊙). Similarly, Figures 11 and 12 show the running integrals for the case of "highly" diffusive and "low" diffusion microporous carbon, respectively. One can observe that for mesoporous and highly diffusive microporous cases, there are wide diffusion channels along certain axes (absence of carbon wall to prevent molecule-wall collisions) that result in significantly anisotropic diffusion. The diffusion along these channels is also large owing to relatively unhindered motion, especially at low concentrations. This is different from the "low" diffusion microporous case, where the pore walls are distributed more homogeneously (in three dimensions), resulting in significant molecule-wall

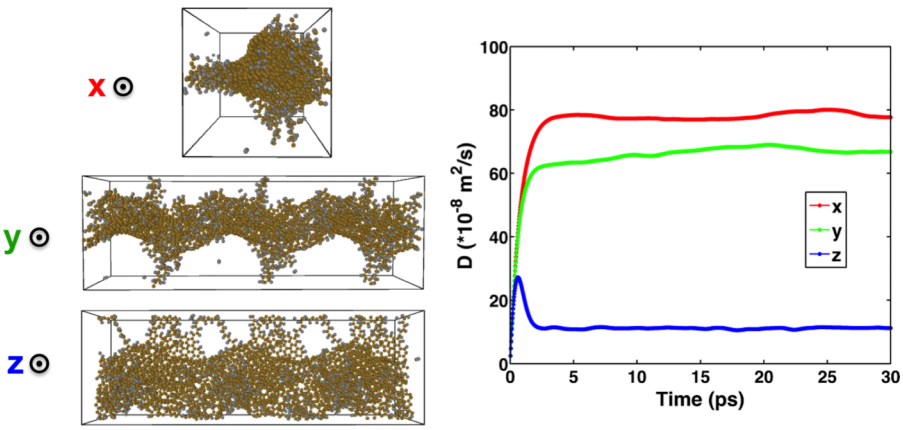

FIG. 10. Anisotropic diffusion in mesoporous carbon (replicated along x axis). Projections of the amorphous carbon structure along different axes (left) and the accompanying diffusion constants. The symbol (⊙) represents axis vector pointing out of the page (normal to the plane).

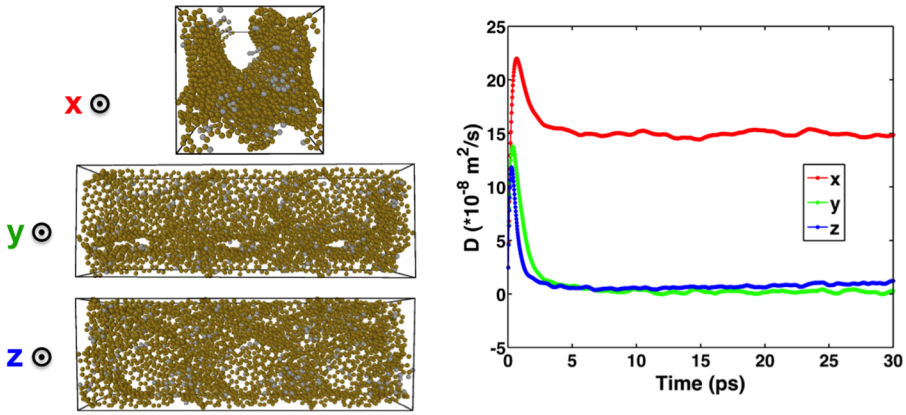

FIG. 11. Anisotropic diffusion in high-diffusion regime microporous carbon. The selective presence of diffusion channels along the x-axis leads to significantly larger diffusion in that direction.

scattering along all three axes. This in turn leads to a relatively isotropic, low diffusion that is largely concentration-independent (Knudsen-like diffusion).

The VACF data and τ_c also enable us to calculate the average flight distance of molecules before back-scattering from the wall. The average velocity of the molecules is taken as the square root of the initial data point of VACF. Assuming an initial ballistic motion, the *average flight distance* to wall, d_{avg} is given to a first approximation by

$$d_{avg} = \sqrt{\langle v(0)v(0)\rangle} \times \tau_c. \tag{4}$$

Shown in Figure 13 is the variation of d_{avg} with concentration of H_2 gas (in terms of number of molecules) for both meso and microporous structures, at 1750 K. For the microporous case, two structures are considered, corresponding to the low and high diffusion regimes as noted before. For comparative purposes, the d_{avg} data are normalized by the d_{avg} at lowest concentration for each case. An interesting observation is that both meso and microporous structures show similar trends with gas concentration, with the mesoporous structure showing d_{avg}, that is, a factor of about 4.5 larger than the low-diffusion microporous structure. Likewise, d_{avg} of mesoporous carbon is about 2.8 times larger than the high-diffusion microporous structure. In other words, the molecules diffusing in mesoporous carbon have to travel larger distances than the microporous case. These factors are also seen to be very close to the ratio of free surface areas (calculated using Zeo++, assuming a spherical pore) for the two cases, which are equal to 4.7 (low diffusion microporous) and 2.6 (high diffusion microporous). This dependence of the average flight distance (to backscattering) on the pore surface areas indicates that the effect of gas-wall collisions is predominant, a characteristic of Knudsen like diffusion behavior.

D. Comparisons with analytically determined Knudsen and normal diffusion

The concentration-independent nature of diffusion in microporous structures hints strongly at a Knudsen diffusion like behavior. For mesoporous diffusion, the concentration-independence begins to appear for lower concentrations. A comparison of the computed diffusivities (MD based) with the analytically prescribed Knudsen and normal diffusivities is presented in this sub-section. The Knudsen diffusivity, D_K[52] for a pore of diameter d_p, and a molecule of mass, M can be obtained according to Eq. (5). This analytical relation leads to the diffusivities (D_K) of the order of (5-20) $\times 10^{-7}$ m^2/s for microporous carbon and about 4.10×10^{-6} m^2/s for mesoporous carbon. These values are lower by a factor of roughly 20-30 for the microporous carbon and 2-3 for the mesoporous carbon (as shown in Figures 9(a) and 9(b)),

$$D_K = \frac{d_p}{3}\sqrt{\frac{8RT}{\pi M}}. \tag{5}$$

Such an over-prediction by Knudsen equation has been observed for gas diffusion in porous media,[15,53] with the error attributed to the incorrect assumption of purely diffuse scattering between the gas and wall. For a more rigorous treatment of Knudsen diffusion, one needs to take into account the surface

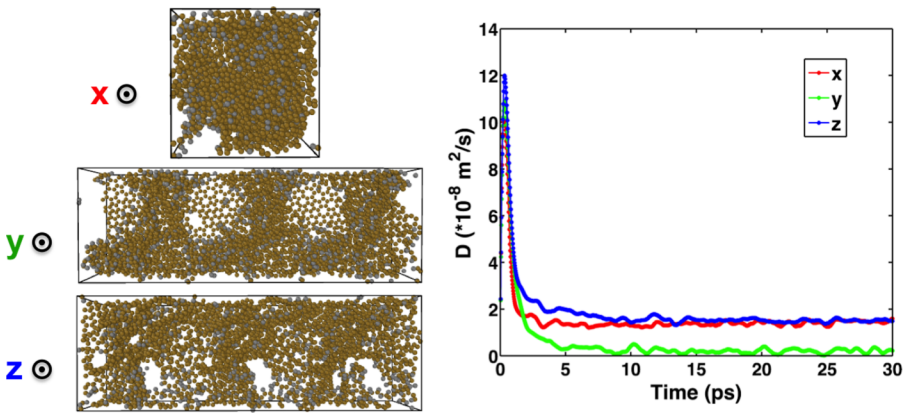

FIG. 12. Diffusion in low-diffusion regime microporous carbon showing greater isotropic diffusion compared to the highly diffusive case (refer Figure 11) owing to more homogeneity in distribution of pore walls along the three axes.

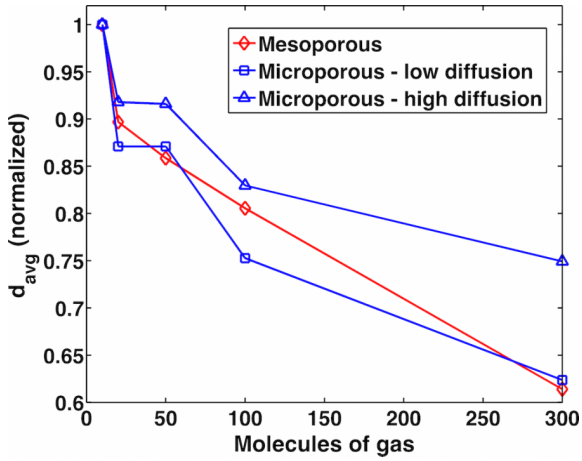

FIG. 13. Variation of normalized average flight distances, d_{avg}, before backscattering from wall for a mesoporous and two microporous structures (low and high diffusion regime structures), as a function of number of molecules of H_2 gas at 1750 K. The actual d_{avg} for each structure was observed to be proportional to the ratio of free surface areas.

roughness and pore tortuosity,[9,20] which are beyond the scope of this work.

In general, the effect of both the gas-gas collisions contributing to the normal (Fickian) diffusivity, D_N and the gas-wall collisions leading to the Knudsen diffusion can be combined in to an interpolation formula known as the "Bosanquet relation"[8] to obtain the effective diffusivity, D_{eff} as per the following:

$$\frac{1}{D_{\text{eff}}} = \frac{1}{D_N} + \frac{1}{D_K}. \tag{6}$$

Applying the Bosanquet relation to the case of H_2 diffusion in microporous carbon leads to D_{eff} of about 70×10^{-8} m^2/s and 120×10^{-8} m^2/s at 1750 K for the highest and lowest concentrations considered, respectively. As in the case of analytically estimated Knudsen diffusivity value, we see the estimation of D_{eff} from Bosanquet relation also over-predicts the simulation results by a factor of 10 to 15 for the low diffusion microporous structure and by a factor of about 3 for the highly diffusive microporous structure. On the other hand, for mesoporous carbon, the Bosanquet relation yields D_{eff} of about 88×10^{-8} m^2/s and 365×10^{-8} m^2/s for the highest and lowest concentrations, which are much closer to the values from simulation (found to be $\sim 160 \times 10^{-8}$ m^2/s and $\sim 331 \times 10^{-8}$ m^2/s, respectively) in comparison to microporous case. The better approximation for the effective diffusivity in mesoporous media simply stems from the fact that as concentration increases, the contribution of Knudsen diffusivity to the Bosanquet relation becomes less significant.

IV. CONCLUSIONS

In the present work, we have studied the mechanism of diffusion of gases in microporous and mesoporous amorphous carbon using molecular dynamics simulations. Porosity and pore connectivity are seen to play a major role in the diffusion characteristics of the gases under consideration. Diffusion in a structure of 1 g/cm^3 density microporous carbon was found to be of the order of (2–40) $\times 10^{-8}$ m^2/s, which is approximately an order of magnitude lower than diffusion in a structure of 0.5 g/cm^3 mesoporous carbon and about two orders of magnitude lower than pure gas diffusion. Using multiple realizations of the structures (11 for the microporous case and 6 for the mesoporous case) generated via the liquid quench method, we compute the self-diffusivity of H_2 molecules at a range of concentrations and temperatures. We observe that for microporous carbon, two scenarios of gas diffusion could arise, depending on the structure—(a) a "highly" diffusive structure where diffusion is predominantly anisotropic due to presence of wide channels for diffusion resulting in significantly high diffusivities ($\sim$20–40 $\times 10^{-8}$ m^2/s). Nine of the eleven structures show this behavior and (b) a "low" diffusion structure (shown by two realizations) that was observed to have a relatively homogeneous distribution of pore features, resulting in low diffusivities that are also relatively isotropic and largely concentration-independent. For both "highly" diffusive microporous carbon and mesoporous carbon (which is anisotropic as well), diffusion was seen to initially increase with a decrease in gas concentration, followed by a very gradual increase as function of inverse concentration. Such a behavior is attributed to significant gas-wall collisions in the case of low-diffusion microporous structure compared to a much weaker contribution of gas-wall collisions for the highly diffusive microporous and mesoporous structures. In addition, for the microporous case, self-diffusivity of various gases like H_2, O_2, H_2O, and CO was computed for the low diffusion structure at different temperatures (350 K–1750 K) and was seen to be nearly independent of gas concentration. We note that the average flight distance of gas molecules before back-scattering from the carbon wall is proportional to the free surface areas, illustrating dominance of Knudsen type gas-wall collisions. It is found that Knudsen relation significantly over-predicts the diffusion estimates for the microporous case, an observation consistent with previous reports. Diffusivities estimated using the Bosanquet relation overestimate for the microporous carbon but provide a good approximation for the mesoporous case. Further, three-dimensional "diffusion maps" that show the simultaneous dependence of diffusion constants on temperature and gas pressure were constructed, which could aid in establishing diffusion constants at arbitrary temperatures and pressures. Such diffusion maps could be used while performing higher-length scale computational fluid dynamics simulations of phenomena involving gas diffusion in porous carbons (reminiscent of ablative char). The study presented from the point of view of structural features of the amorphous carbon is expected to hold true for other micro and mesoporous amorphous structures and could aid in prediction of concentration dependence of diffusivities.

ACKNOWLEDGMENTS

This work was sponsored by U.S. Navy–Naval Air Warfare Center Weapons Division (NAWCWD) through a Small Business Technology Transfer (STTR) grant, Contract No. N68335-13-C-0119, awarded to Advanced Cooling Technologies, Inc., (ACT) based in Lancaster, Pennsylvania. All work reported here was undertaken at ACT. The simulations reported in this work made use of computing time provided by NAWCWD, at the Spirit (AFRL) supercomputer. Valuable

suggestions from Professor Donald Brenner of North Carolina State University are acknowledged.

[1]J. R. Li, R. J. Kuppler, and H. C. Zhou, "Selective gas adsorption and separation in metal-organic frameworks," Chem. Soc. Rev. **38**, 1477–1504 (2009).
[2]E. D. Bloch, W. L. Queen, R. Krishna, J. M. Zadrozny, C. M. Brown, and J. R. Long, "Hydrocarbon separations in a metal-organic framework with open iron(II) coordination sites," Science **335**, 1606–1610 (2012).
[3]R. E. Cunningham and R. J. J. Williams, *Diffusion in Gases and Porous Media* (Plenum Press, New York, 1980).
[4]A. I. Skoulidas, D. M. Ackerman, J. K. Johnson, and D. S. Sholl, "Rapid transport of gases in carbon nanotubes," Phys. Rev. Lett. **89**, 185901-1–185901-4 (2002).
[5]A. I. Skoulidas and D. S. Sholl, "Self-diffusion and transport diffusion of light gases in metal-organic framework materials assessed using molecular dynamics simulations," J. Phys. Chem. B **109**, 15760–15768 (2005).
[6]A. I. Skoulidas and D. S. Sholl, "Transport diffusivities of CH_4, CF_4, He, Ne, Ar, Xe, and SF_6 in silicalite from atomistic simulations," J. Phys. Chem. B **106**, 5058–5067 (2002).
[7]R. J. Millington, "Gas diffusion in porous media," Science **130**, 100–102 (1959).
[8]R. B. Evans and G. M. Watson, "Gaseous diffusion in porous media," J. Chem. Phys. **35**, 2076–2083 (1961).
[9]S. K. Bhatia and D. Nicholson, "Modeling mixture transport at the nanoscale: Departure from existing paradigms," Phys. Rev. Lett. **100**, 236103-1–236103-4 (2008).
[10]P. J. A. M. Kerkhof and M. A. M. Geboers, "Analysis and extension of the theory of multicomponent fluid diffusion," Chem. Eng. Sci. **60**, 3129–3167 (2005).
[11]R. Krishna, "Describing the diffusion of guest molecules inside porous structures," J. Phys. Chem. C **113**, 19756–19781 (2009).
[12]R. Krishna, "Diffusion in porous crystalline materials," Chem. Soc. Rev. **41**, 3099–3118 (2012).
[13]R. Ryoo, S. H. Joo, M. Kruk, and M. Jaroniec, "Ordered mesoporous carbons," Adv. Mater. **13**, 677–681 (2001).
[14]A. I. Skoulidas, D. S. Sholl, and R. Krishna, "Correlation effects in diffusion of CH_4/CF_4 mixtures in MFI zeolite. A study linking MD simulations with the Maxwell-Stefan formulation," Langmuir **19**, 7977–7988 (2003).
[15]R. Krishna and J. M. van Baten, "A molecular dynamics investigation of the unusual concentration dependencies of Fick diffusivities in silica mesopores," Microporous Mesoporous Mater. **138**, 228–234 (2011).
[16]J. M. D. MacElroy and K. Raghavan, "Adsorption and diffusion of a Lennard-Jones vapor in microporous silica," J. Chem. Phys. **3**, 2068–2079 (1990).
[17]M. Sahimi and V. L. Jue, "Diffusion of large molecules in porous media," Phys. Rev. Lett. **62**, 629–632 (1989).
[18]S. Y. Lim, T. T. Tsotsis, and M. Sahimi, "Molecular simulation of diffusion and sorption of gases in an amorphous polymer," J. Chem. Phys. **119**, 496–504 (2003).
[19]J. D. Moore, J. C. Palmer, Y. C. Liu, T. J. Roussel, J. K. Brennan, and K. E. Gubbins, "Adsorption and diffusion of argon confined in ordered and disordered microporous carbons," Appl. Surf. Sci. **256**, 5131–5136 (2010).
[20]K. Malek and M. O. Coppens, "Effects of surface roughness on self- and transport diffusion in porous media in the Knudsen regime," Phys. Rev. Lett. **87**, 125505 (2001).
[21]S. Jiang, K. E. Jelfs, D. Holden, T. Hasell, S. Y. Chong, M. Haranczyk, A. Trewin, and A. I. Cooper, "Molecular dynamics simulations of gas selectivity in amorphous porous molecular solids," J. Am. Chem. Soc. **135**, 17818–17830 (2013).
[22]E. J. Maginn, A. T. Bell, and D. N. Theodorou, "Transport diffusivity of methane in silicalite from equilibrium and nonequilibrium simulations," J. Phys. Chem. **97**, 4173–4181 (1993).
[23]D. S. Sholl, "Understanding macroscopic diffusion of adsorbed molecules in crystalline nanoporous materials via atomistic simulations," Acc. Chem. Res. **39**, 403–411 (2006).
[24]G. Walberg, "Analytical study of diffusion-controlled char oxidation and its effect on steady-state ablation of plastic materials," NASA Technical Report (TR R-242), 1966.
[25]J. Shen and J. M. Smith, "Diffusional effects in gas-solid reactions," Ind. Eng. Chem. Fundam. **4**, 293–301 (1965).
[26]K. Ding and H. Andersen, "Molecular-dynamics simulation of amorphous germanium," Phys. Rev. B **34**, 6987–6991 (1986).
[27]A. C. T. van Duin, S. Dasgupta, F. Lorant, and W. A. Goddard III, "ReaxFF: A reactive force field for hydrocarbons," J. Phys. Chem. A **105**, 9396–9409 (2001).
[28]N. Marks, "Modelling diamond-like carbon with the environment-dependent interaction potential," J. Phys.: Condens. Matter **14**, 2901–2926 (2006).
[29]J. C. Palmer, A. Llobet, S. H. Yeon, J. E. Fischer, Y. Shi, Y. Gogotsi, and K. E. Gubbins, "Modeling the structural evolution of carbide-derived carbons using quenched molecular dynamics," Carbon **48**, 1116–1123 (2010).
[30]Y. Shi, "A mimetic porous carbon model by quench molecular dynamics simulation," J. Chem. Phys. **128**, 234707-1–234707-11 (2008).
[31]S. Bhattacharya and J. Kieffer, "Fractal dimensions of silica gels generated using reactive molecular dynamics simulations," J. Chem. Phys. **122**, 094715-1–094715-8 (2005).
[32]J. Rosen, O. Warschkow, D. R. McKenzie, and M. M. M. Bilek, "Amorphous and crystalline phases in thermal quench simulations of alumina," J. Chem. Phys. **126**, 204709-1–204709-9 (2007).
[33]K. Chenoweth, A. C. T. van Duin, and W. A. Goddard III, "ReaxFF reactive force field for molecular dynamics simulations of hydrocarbon oxidation," J. Phys. Chem. A **112**, 1040–1053 (2008).
[34]S. G. Srinivasan and A. C. T. van Duin, "Molecular-dynamics-based study of the collisions of hyperthermal atomic oxygen with graphene using the ReaxFF reactive force field," J. Phys. Chem. A **115**, 13269–13280 (2011).
[35]K. D. Nielson, A. C. T. van Duin, J. Oxgaard, W. Q. Deng, and W. A. Goddard III, "Development of the ReaxFF reactive force field for describing transition metal catalyzed reactions, with application to the initial stages of the catalytic formation of carbon nanotubes," J. Phys. Chem. A **109**, 493–499 (2005).
[36]L. D. Gelb and K. E. Gubbins, "Characterization of porous glasses: Simulation models, adsorption isotherms, and the Brunauer-Emmett-Teller analysis method," Langmuir **14**, 2097–2111 (1998).
[37]J. Pikunic, C. Clinard, N. Cohaut, K. E. Gubbins, J. M. Guet, R. J.-M. Pellenq, I. Rannou, and J.-N. Rouzaud, "Structural modeling of porous carbons: Constrained reverse Monte Carlo method," Langmuir **19**, 8565–8582 (2003).
[38]S. K. Jain, R. J. -M. Pellenq, J. P. Pikunic, and K. E. Gubbins, "Molecular modeling of porous carbons using the hybrid reverse Monte Carlo method," Langmuir **22**, 9942–9948 (2006).
[39]J. C. Palmer and K. E. Gubbins, "Atomistic models for disordered nanoporous carbons using reactive force fields," Microporous Mesoporous Mater. **154**, 24–37 (2012).
[40]R. Ranganathan, S. Rokkam, T. Desai, and P. Keblinski, "Generation of realistic amorphous carbon models using liquid quench method" (unpublished).
[41]T. F. Willems, C. H. Rycroft, M. Kazi, J. C. Meza, and M. Haranczyk, "Algorithms and tools for high-throughput geometry-based analysis of crystalline porous materials," Microporous Mesoporous Mater. **149**, 134–141 (2012).
[42]See supplementary material at http://dx.doi.org/10.1063/1.4928633 for (a) visualization of amorphous carbon structures generated in this work see Figures S1 to S3 and (b) for evidence on lack of gas adsorption in the model amorphous carbon structures see Figure S4.
[43]H. Sun, S. J. Mumby, J. R. Maple, and A. T. Hagler, "An *ab initio* CFF93 all-atom force field for polycarbonates," J. Am. Chem. Soc. **116**, 2978–2987 (1994).
[44]S. Plimpton, "Fast parallel algorithms for short-range molecular dynamics," J. Comput. Phys. **117**, 1–19 (1995).
[45]D. Frenkel and B. Smit, *Understanding Molecular Simulation: From Algorithms to Applications* (Academic Press, 2002).
[46]S. Jakobtorweihen, M. G. Verbeek, C. P. Lowe, F. J. Keil, and B. Smit, "Understanding the loading dependence of self-diffusion in carbon nanotubes," Phys. Rev. Lett. **95**, 044501 (2005).
[47]G. D. Bergland, "A guided tour of the fast Fourier transform," IEEE Spectrum **6**, 41–52 (1969).
[48]S. P. Nunes, R. A. da Costa, S. P. Barbosa, and G. R. Almeida, "Tracking degradation and pyrolysis of EPDM insulators," IEEE Trans. Electr. Insul. **24**, 99–105 (1989).
[49]T. G. Desai, S. K. Rokkam, R. Ranganathan, D. Brenner, P. Keblinski, and R. Vander Wal, "Methodology development of atomistically-informed chemical kinetics model for rubber composite materials," NAVAIR STTR Phase II (Base) Final Report, Contract No. N68335-13-C-0119, Distribution B: Distribution authorized to US Government Agencies Only, 30 July 2014.
[50]B. Smit and T. L. M. Maesen, "Molecular simulations of zeolites: Adsorption, diffusion, and shape selectivity," Chem. Rev. **108**, 4125–4184 (2008).
[51]M.-O. Coppens, A. T. Bell, and A. K. Chakraborty, "Dynamic Monte-Carlo and mean-field study of the effect of strong adsorption sites on self-diffusion in zeolites," Chem. Eng. Sci. **54**, 3455–3463 (1999).
[52]J. Karger, D. M. Ruthven, and D. N. Theodorou, *Diffusion in Zeolites and Other Nanoporous Materials* (Wiley-VCH, Weinheim, 2012).
[53]S. K. Bhatia and D. Nicholson, "Some pitfalls in the use of the Knudsen equation in modelling diffusion in nanoporous materials," Chem. Eng. Sci. **66**, 284–293 (2011).